Eur. Phys. J. A **9**, 29–34 (2000)

THE EUROPEAN PHYSICAL JOURNAL A

Magnetic properties of the $\nu j_{15/2}$ intruder orbital in the superdeformed minimum of ^{197}Pb

N. Buforn[1], A. Astier[1,a], R. Duffait[1], M. Meyer[1], S. Perriès[1], A. Prévost[1], N. Redon[1], O. Stézowski[1], A. Goergen[2], H. Hübel[2], E. Mergel[2], S. Neumann[2], D. Rossbach[2], N. Nenoff[2], G. Schoenwasser[2], A. Bauchet[3], I. Deloncle[3], M.G. Porquet[3], A.N. Wilson[4], R. Lucas[5], F.A. Beck[6], D. Curien[6], G. Duchêne[6], B.J.P. Gall[6], N. Kintz[6], J.P. Vivien[6], and D.M. Cullen[7]

[1] IPN Lyon, IN2P3/CNRS, Université Lyon-1, F-69622 Villeurbanne Cedex, France
[2] Institut für Strahlen- und Kernphysik, Universität Bonn, Nussallee 14-16, D-53115 Bonn, Germany
[3] CSNSM Orsay, IN2P3/CNRS, Université Paris-Sud, F-91405 Orsay Campus, France
[4] Department of Physics, University of York, York Y01 5DD, UK
[5] CEA/Saclay, DAPNIA/SPhN, F-91191 Gif-sur-Yvette, France
[6] IReS Strasbourg, IN2P3/CNRS, Université Louis Pasteur, F-67037 Strasbourg, France
[7] Oliver Lodge Laboratory, Department of Physics, University of Liverpool, Liverpool L69 7ZE, UK

Received: 14 June 2000 / Revised version: 29 August 2000
Communicated by D. Schwalm

Abstract. This work has established eight cross-talk transitions between the two signature partner superdeformed (SD) bands in ^{197}Pb with the EUROBALL IV spectrometer. Directional correlations from oriented states measurements confirm the $\Delta I = 1$ character of these transitions. The flat behaviour of the dynamical moment of inertia and the agreement between the experimental and microscopic HF+BCS values of $(g_K - g_R)\, K/Q_0$ suggest that the configuration of the SD bands is based upon the $\nu[752]5/2^-$ neutron intruder orbital. The derived effective spin gyromagnetic factor $g_s^{\rm eff}$ is found to be not quenched, and is close to the theoretical $g_s^{\rm free}$ value.

PACS. 21.10.Re Collective levels – 23.20.En Angular distribution and correlation measurements – 23.20.Lv Gamma transitions and level energies – 27.80.+w $190 \leq A \leq 219$

1 Introduction

Since the prediction of a superdeformed (SD) minimum in the nuclear potential energy surface in the $A = 190$ mass region by both microscopic and macroscopic calculations [1–5], about 70 SD bands have been discovered in 25 nuclei of this mass region [6]. Most of the SD bands show a smooth increase of the dynamical moment of inertia $\Im^{(2)}$ with increasing rotational frequency. As first discussed in ref. [7], this typical rise is well-explained by the gradual alignments of quasineutrons and quasiprotons coming from high-N intruder orbitals ($\nu j_{15/2}$ and $\pi i_{13/2}$, respectively), combined with a reduction of the pairing. This interpretation is confirmed by the observation of a flat dynamical moment of inertia behaviour for several bands in odd-mass Pb and Hg, and in odd-odd Tl nuclei. Indeed, since the corresponding configurations involve the occupation of the intruder orbitals, the quasiparticle alignment is prevented by Pauli blocking. Going further, the double blocking (neutron and proton) observed in the odd-odd Tl isotopes shows that when increasing the frequency, the alignment of quasineutrons occurs first and is completed at a frequency ~ 0.3 MeV, whereas the alignment of quasiprotons is starting at this frequency [8].

Another interesting phenomenon is the cross-talk between SD bands. Indeed, SD bands built on high-K configurations should show strong M1 transitions between two signature partners in the strong coupling scheme. Such M1 cross-talk transitions have been observed experimentally only in five nuclei in the $A = 190$ mass region (^{193}Hg [9], ^{191}Tl [10], ^{193}Tl [11], ^{195}Tl [12], and ^{193}Pb [13,14]). The extraction of $B(\mathrm{M1})/B(\mathrm{E2})$ ratios between two SD signature partners allows the assignment of precise configurations and gives access to the magnetic properties of the SD states.

The isotope ^{197}Pb was investigated some years ago with the EUROGAM II γ-ray spectrometer array, when two SD bands were observed in this nucleus [15]. On the basis of the behaviour of the dynamical moments of inertia, these two bands have been interpreted as the two signatures of the $\nu[752]5/2$ intruder orbital. Moreover, as the two bands were observed in coincidence with each other, they were good candidates to search for M1 cross-

[a] e-mail: astier@ipnl.in2p3.fr

talk transitions with the high detection efficiency provided by the EUROBALL IV spectrometer [16]. In the present work we report the observation of these M1 transitions, allowing to extract for the first time the magnetic properties of the neutron $j_{15/2}$ intruder orbital in the SD well.

2 Experiment and data analysis

High spin states of ^{197}Pb have been populated via the ^{186}W(^{18}O,7n)^{197}Pb reaction. A stack of $2 \times 200\mu$g/cm^2 of ^{186}W foils were bombarded by 117 MeV ^{18}O delivered by the Vivitron accelerator in Strasbourg. The γ-ray transitions were measured with the EUROBALL IV array [16] which consists of 239 Ge crystals. More precisely, EUROBALL IV comprises i) 30 tapered Ge detectors placed on three rings at forward angles, ii) 26 clover detectors each composed of 4 Ge crystals in the same cryostat at angles close to 90°, iii) 15 cluster detectors formed by 7 Ge capsules at backward angles, and iv) an inner-ball composed of 210 BGO crystals. All the Ge detectors are surrounded by BGO scintillators used for Compton suppression. The detector signals are processed through VXI electronics which sends the data to three event collectors. Finally, a processor farm builds the EUROBALL event recorded on DLT tapes. A condition of four unsuppressed Ge detectors firing in coincidence combined with an inner-ball multiplicity of 8 was required to start the acquisition. After presorting the raw data (prompt time window, add-back of clover and cluster composite detectors, Compton rejection), a total of 10^9 four- and higher-fold events have finally been analyzed.

The knowledge of the efficiency at low energy (in the 100–250 keV range) is crucial for a correct extraction of the intensities. However, it is well-known that an efficiency obtained from source data cannot be applied in this low-energy range for high-fold data. Indeed, due to their longer detection time, low-energy transitions may not be in the prompt coincidence time window, and therefore, they will not be counted in the event. Thus, the efficiency obtained with sources overestimates the real high-fold efficiency at low energies. The relative high-fold efficiency has been established using low-energy quadrupole transitions of ^{194,195}Hg produced in the reaction. We obtain the efficiency by applying the intensity conservation rule in a γ-ray cascade gated from above to exclude the side-feeding. We observe a reduction of $\sim 30\%$ at 100 keV.

Multiconditioned one-dimensional spectra and gated matrices have been constructed during the data analysis. All histograms have been incremented taking into account the intensity problems first pointed out in ref. [17], which can lead to unphysical spikes discussed in ref. [18]. To extract the SD bands, it has been necessary to build spectra with at least three gates and a proper background subtraction.

Directional Correlations from Oriented states (DCO) matrices have been built and DCO ratios have been extracted using the EUROBALL IV geometry presented in fig. 1. By taking into account the angular symmetries of the correlation function $W(\theta_1, \theta_2, \Delta\phi = \phi_2 - \phi_1)$ [19],

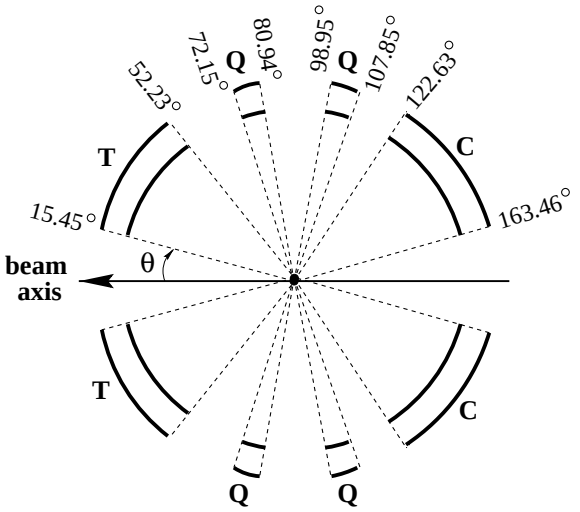

Fig. 1. Schematic angular geometry of the EUROBALL IV array showing the tapered (T), clover (Q) and cluster (C) groups of detectors. Limiting angles are indicated with respect to the beam axis.

the $C^2_{239} = 28441$ combinations of 2 detectors on EUROBALL IV could be reduced to 15744 distinct geometries. Of course we have not looked at these individual geometries for lack of statistics. Instead we have separated the detectors of the EUROBALL IV array into two sets: one with the clover (Q) detectors (located around 90° with respect to the beam axis), and another with all tapered (T) and cluster (C) detectors, located at forward and backward angles, respectively.

By noting $W(\text{det1}, \text{det2}) = W(\theta_1, \theta_2, \Delta\phi)$ the correlation function between the two detectors det1 and det2 at angles (θ_1, ϕ_1) and (θ_2, ϕ_2), we define the two average correlation functions:

$$W(\mathrm{T}+\mathrm{C}, \mathrm{Q}) = \sum_{\text{det1} \in \{\mathrm{T}+\mathrm{C}\}} \sum_{\text{det2} \in \{\mathrm{Q}\}} \frac{W(\text{det1}, \text{det2})}{N_{\text{comb}}},$$

$$W(\mathrm{Q}, \mathrm{T}+\mathrm{C}) = \sum_{\text{det1} \in \{\mathrm{Q}\}} \sum_{\text{det2} \in \{\mathrm{T}+\mathrm{C}\}} \frac{W(\text{det1}, \text{det2})}{N_{\text{comb}}},$$

where N_{comb} is the number of distinct pairs (T+C,Q), *i.e.* the number of tapered and cluster segments, multiplied by the number of clover crystals. Then, a "generalized" DCO ratio can be defined by

$$R_{\text{DCO}} = \frac{W(\mathrm{T}+\mathrm{C}, \mathrm{Q})}{W(\mathrm{Q}, \mathrm{T}+\mathrm{C})}.$$

The theoretical DCO ratio derived for this geometry has been calculated for a cascade $I_1 \rightarrow I_2 \rightarrow I_3$, starting from a completely aligned state with $I_1 = 21/2$. For each pair (T+C,Q), the corresponding value lies in the interval $[0.41, 0.80]$ for a stretched dipole-quadrupole sequence, depending on the detector pair considered, and the average value is $\overline{R_{\text{DCO}}} = 0.55$. It is therefore easily distinguishable from any stretched quadrupole-quadrupole sequence which has a DCO ratio of 1.00. This procedure

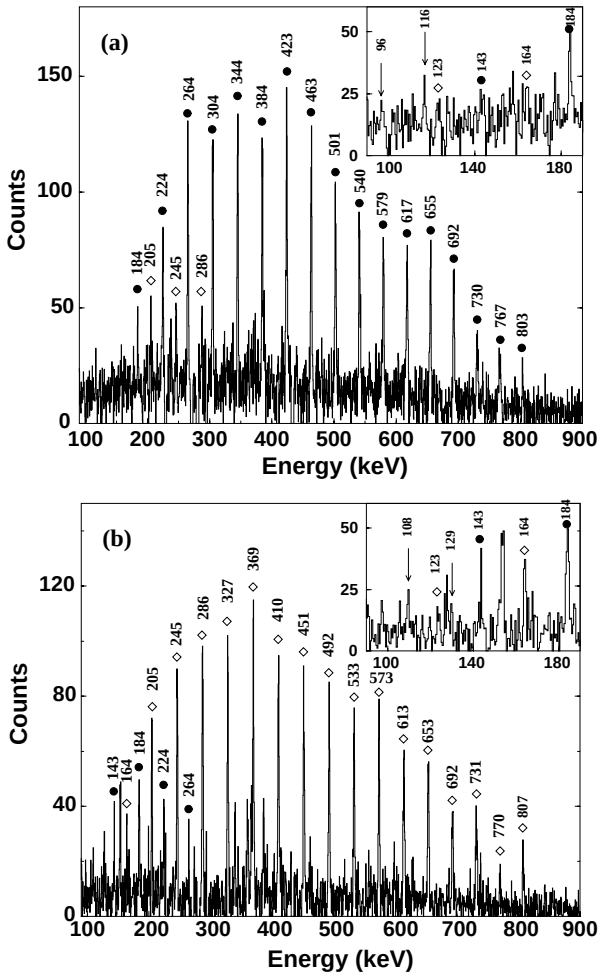

Fig. 2. Quadruple gated spectrum on (a) SD1 (4 gates among the following transitions: 304, 344, 384, 423, 463, 501, 540, 579, 617, 655, 692, and 730 keV), and (b) SD2 of ^{197}Pb (4 gates among the following transitions: 286, 327, 369, 410, 451, 492, 533, 573, 613, 653, 692, 731 and 770 keV), showing the cross-talk between SD1 (filled circles) and SD2 (open diamonds). In the low-energy part of the spectra displayed in inserts, the new SD transitions are labeled with their energies and the cross-talk transitions between SD1 and SD2 are indicated with arrows.

has been checked with cascades of transitions with known multipolarities of low-lying normal deformed (ND) states [20]. It was also successfully applied to a previous study performed with EUROBALL III for the decay-out of the ^{136}Nd SD band [21].

3 Results

Firstly we confirm the presence of the two SD bands initially discovered by Hibbert *et al.* in ^{197}Pb [15], as shown in the spectra of figs. 2(a) and 2(b). The two spectra have been obtained by requiring at least four gates in the corresponding SD band, excluding the lowest transitions, *i.e.* down to 304 keV for SD1 and 286 keV for SD2. The two bands are weakly populated, about 0.2% compared with the $17/2^+ \rightarrow 13/2^+$ 1005-keV yrast ND transition.

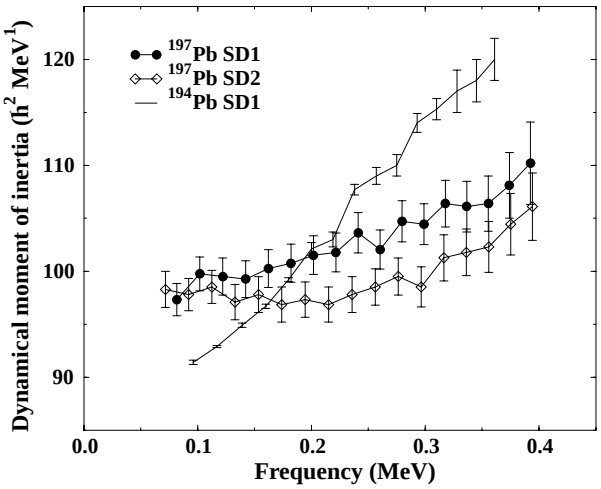

Fig. 3. Dynamical moments of inertia of the two SD bands in ^{197}Pb. For comparison the dynamical moment of inertia of the yrast SD band in ^{194}Pb (from ref. [6]) is also plotted.

There is a slight difference in the transition energies measured in our experiment which are systematically lower by ≈ 0.7 keV compared with the results of ref. [15] (see table 1), whereas, in the same energy range, the low-lying ND transition energies have been found identical to the ones measured by Baldsiefen *et al.* [20].

The two SD bands have been extended to lower frequencies. We suggest that the 143-keV transition is the lowest observed transition below the 184-keV one for SD1, and we add two more transitions for SD2 below the 205-keV transition with energies of 123 keV and 164 keV. These three new SD transitions can be seen in figs. 2(a) and 2(b). Whereas there is no doubt concerning the 164-keV transition, the 143-keV transition is more tentative as well as is the evidence for the 123-keV transition, the latter being much weaker and visible only in certain coincidence spectra.

From the transition energies, we obtain the dynamical moments of inertia $\Im^{(2)}$ of the two SD bands shown in fig. 3. The new SD transitions extend the $\Im^{(2)}$ to lower frequencies, and no significant change in their behaviour is observed. The moments of inertia of the two SD bands remain flat at lower frequencies, at a value around 98 $\hbar^2$MeV^{-1}.

The spins of the SD levels have been obtained using the spin fit method [22] from a conventional Harris fit of the moment of inertia [23]. The values are in accordance with the ones obtained by the method of Wu *et al.* [24]. The spins of the lowest SD states are then proposed to be $(11/2^-)$ for SD1 and $(9/2^-)$ for SD2 (see fig. 4). It is worth noting that the two bands are observed down to very low spins, close to the $K = 5/2$ SD bandhead, and to lower spins than the $13/2^+$ isomeric state of ^{197}Pb.

The figures 2(a) and 2(b) clearly demonstrate the cross-talk between the two SD bands, and the mid-point energy pattern, which is typical of strongly coupled signature partners, can be seen between the two bands. The 164-, 205-, 245- and 286-keV transitions appear in

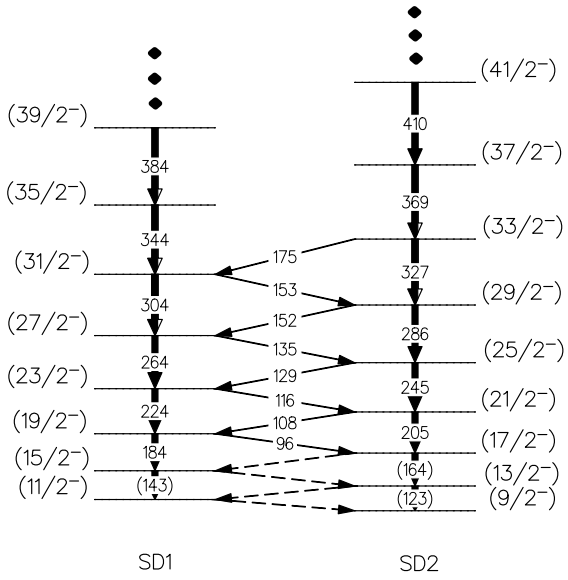

Fig. 4. Cross-talk level scheme of the two SD bands of ^{197}Pb, signature partners of the [752]5/2 orbital.

coincidence with SD1, and conversely the 143-, 184-, 224- and 264-keV transitions appear in coincidence with SD2. Furthermore, by gating at higher energies in the two SD bands, we have now established that the cross-talk is present for a rather large range of transition energies: up to the 327-keV SD2 transition in the SD1 spectrum, and up to the 344-keV SD1 transition in the SD2 spectrum. The splitting between the two orbitals is thus occurring at a frequency of ≈ 0.17 MeV.

Cross-talk transitions between the two SD bands must be searched in the low-energy part of figs. 2(a) and 2(b) which are enlarged in the inserts. The 96- and 116-keV transitions are in coincidence with SD1, whereas the 108- and 129-keV transitions are in coincidence with SD2. These transitions have been confirmed and other new candidates have been found in a meticulous search for coincidence relationships between the top of one SD band and the bottom of the other, selecting one given path between the two bands. Despite the low statistics in these spectra, we have observed the eight following inter-band transitions between the two SD bands: 96, 108, 116, 129, 135, 152, 153 and 175 keV. The energy sum rules between the SD transitions and these new cross-talk transitions are fulfilled with a maximum deviation of 0.5 keV. One should mention that the observation of the 96- and 116-keV transitions on the one hand, and of the 108- and 129-keV transitions on the other, is enhanced by the gating conditions used to obtain the spectra of figs. 2(a) and 2(b). The other cross-talk transitions are more evident in spectra built with fewer low-energy gates in the SD bands. Therefore, we propose that the two SD bands in ^{197}Pb follow the cross-talk scheme presented in fig. 4.

The spins proposed in fig. 4 have been obtained by DCO measurements of the cross-talk and the SD intraband transitions. These DCO values are summarized in table 1 and are plotted in fig. 5. As shown, all measurable

Table 1. Experimental DCO ratios for SD and cross-talk transitions of ^{197}Pb (see text for explanation of the method). A missing DCO value means that the measurement was impossible because of a too weak intensity (a) or contamination (b) for the corresponding transition.

SD1 transition (keV)	DCO ratio	SD2 transition (keV)	DCO ratio
142.6 (5)	(a)	123.0 (5)	(a)
183.7 (4)	1.10 (14)	163.7 (5)	0.99 (28)
223.8 (5)	1.10 (13)	204.6 (4)	1.06 (20)
264.0 (5)	1.13 (17)	245.2 (5)	1.09 (13)
304.3 (5)	1.08 (12)	286.4 (5)	1.06 (12)
344.2 (5)	1.00 (11)	327.3 (5)	1.02 (12)
383.9 (5)	1.04 (15)	368.6 (5)	1.15 (9)
423.3 (5)	1.08 (15)	409.7 (5)	0.97 (15)
462.6 (5)	1.24 (30)	451.0 (5)	0.98 (16)
501.2 (5)	0.94 (15)	491.9 (5)	1.01 (18)
540.4 (5)	1.02 (15)	532.5 (5)	1.06 (23)
578.6 (5)	1.03 (15)	572.7 (5)	1.10 (25)
616.9 (5)	1.06 (20)	613.3 (6)	0.99 (21)
654.5 (6)	1.10 (24)	652.8 (6)	1.02 (25)
692.2 (6)	(a)	692.1 (6)	1.02 (24)
729.8 (7)	(a)	731.2 (7)	(a)
766.8 (8)	(a)	769.5 (8)	(a)
803.1 (10)	(a)	807.2 (8)	(a)

Cross-talk transition (keV)	DCO ratio
96.4 (4)	(a)
108.5 (4)	0.75 (29)
115.8 (5)	0.65 (21)
129.0 (4)	0.79 (33)
134.8 (5)	(a)
151.9 (6)	(b)
152.6 (6)	(b)
174.6 (5)	(a)

SD transitions are $\Delta I = 2$ (E2) transitions. Concerning the new SD transitions, only the 164-keV transition could be analyzed, the 123- and 143-keV transitions being much weaker (for two complementary reasons: the bands certainly decay towards ND states and the conversion electron process strongly dominates for these low-energy transitions compared with radiative emission). The 164-keV transition is compatible with stretched quadrupole (E2) multipolarity, allowing the extension of the SD band to lower frequency.

Concerning the cross-talk transitions, the three DCO values extracted from non contaminated transitions are compatible with a $\Delta I = 1$ assignment despite the large uncertainties (see table 1 and fig. 5). Under the assumption that the two bands are signature partners, the only possibility is that the cross-talk transitions have M1 multipolarity.

Finally, $B(\mathrm{M1})/B(\mathrm{E2})$ branching ratios have been determined for several states of the two SD bands. Two methods have been used: i) directly from the intensities of the M1 and E2 transitions deexciting the considered levels (with the same method as used in ref. [13]), and

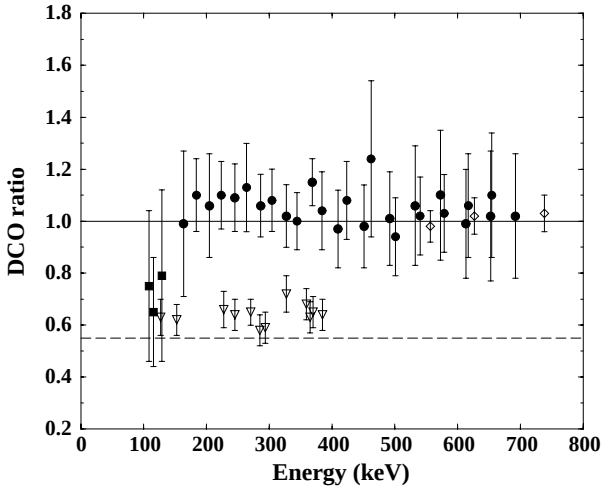

Fig. 5. Experimental DCO ratios for SD1 and SD2 (filled circles) and SD1-SD2 cross-talk (filled squares) transitions. For comparison, experimental DCO ratios extracted in this work are plotted for several known $\Delta I = 2$ (open diamonds) and $\Delta I = 1$ (open triangles) ND transitions of ^{197}Pb. The solid and dashed lines correspond to the theoretical DCO values of the stretched quadrupole-quadrupole and dipole-quadrupole sequences, respectively.

ii) indirectly from the two parallel E2 transitions of each SD band, by knowing the M1 transition energies and applying the conservation rule of the total intensity (in this case electron conversion is taken into account; see for instance refs. [12,14] for more details). The average value $B(\mathrm{M1})/B(\mathrm{E2}) = 0.046 \pm 0.010\ {\mu_N}^2/(\mathrm{eb})^2$ has been obtained for the two SD bands.

4 Discussion

A striking feature of these results concerns the tentative value $(9/2^-)$ of the lowest SD state observed in ^{197}Pb. This is the lowest spin ever observed for an odd SD nucleus of the $A = 190$ mass region. This can be correlated with the fact that the predicted well depth of the secondary minimum increases as the mass number, leading to a higher barrier between the SD and ND wells. The SD well depths predicted in lattice microscopic HF+BCS calculations for even Pb isotopes using the effective force SkM* are: 0.93 MeV for ^{192}Pb, 1.73 MeV for ^{194}Pb, 2.17 MeV for ^{196}Pb, 2.59 MeV for ^{198}Pb and 3.10 MeV for ^{200}Pb [5]. Experimentally, the lowest spin values of the SD bands of odd Pb isotopes have been determined as 17/2 for ^{193}Pb [13], 13/2 for ^{195}Pb [25] and 9/2 for ^{197}Pb. The corresponding values are higher in Hg and Tl isotopes. A linear relation seems to exist between the spin of the lowest observed SD state and the SD well depth. However, it is important to note that our results on ^{197}Pb have been obtained with EUROBALL IV which is more efficient than the two previous arrays used for the ^{193}Pb and ^{195}Pb studies. The resolving powers of the detection arrays should certainly be taken into account.

Table 2. Prediction of the $(g_K - g_R)K/Q_0$ ratio (in $(\mathrm{eb})^{-1}$) using HF+BCS calculations for different neutron valence orbitals in ^{196,198}Pb [26], compared with the experimental average value extracted in this work.

Nucleus	$\nu[505]11/2$	$\nu[761]3/2$	$\nu[642]3/2$
^{196}Pb	−0.191	−0.080	0.001
^{198}Pb	−0.189	−0.080	0.001
^{197}Pb (exp.)	−0.100 (11)	−0.114 (13)	−0.114 (13)

Nucleus	$\nu[512]5/2$	$\nu[752]5/2$	$\nu[624]9/2$
^{196}Pb	−0.128	−0.109	−0.168
^{198}Pb	−0.128	−0.108	−0.165
^{197}Pb (exp.)	−0.112 (12)	−0.112 (12)	−0.106 (12)

As mentioned in the introduction, there were only five cases in the $A = 190$ mass region where $B(\mathrm{M1})/B(\mathrm{E2})$ ratios between two SD signature partners had been measured [9–14]. For proton configuration, only one orbital is involved ($\pi[642]5/2^+$), whereas two neutron orbitals could be analyzed ($\nu[624]9/2^+$ and $\nu[512]5/2^-$).

In the framework of the strong-coupling rotor plus quasiparticle model, the $B(\mathrm{M1})/B(\mathrm{E2})$ branching ratio is expressed as (for $K \neq 1/2$):

$$\frac{B(\mathrm{M1})}{B(\mathrm{E2})} = \frac{\frac{3}{4\pi}\left(\frac{e\hbar}{2Mc}\right)^2 \langle\, I\, K\, 1\, 0 | I{-}1\, K\,\rangle^2}{\frac{5}{16\pi} e^2 \langle\, I\, K\, 2\, 0 | I{-}2\, K\,\rangle^2} \frac{(g_K - g_R)^2\, K^2}{Q_0^2}. \quad (1)$$

Perrièes *et al.* [26] have studied the collective gyromagnetic ratios g_R of even SD $A = 190$ nuclei within the Inglis cranking approximation using microscopic HF+BCS calculations with the effective interaction SkM*. They are found to be very different from the Z/A estimates, smaller by about 30% than this global ansatz. Recently, direct measurements of g factors have been performed in three SD bands of ^{194}Hg [27]. The experimental value $g = 0.36(10)$ obtained for the yrast SD band is in excellent agreement with the theoretical predictions.

In ref. [26], predictions of the $(g_K - g_R)K/Q_0$ ratio have been made for Hg and Pb nuclei, and for ^{196,198}Pb the predictions are given in table 2. From our measured $B(\mathrm{M1})/B(\mathrm{E2})$ ratios in ^{197}Pb, we can now compare the experimental average value of $(g_K - g_R)K/Q_0$ with the calculations. As shown in table 2, the extracted values of $(g_K - g_R)K/Q_0$ exclude low-K (3/2) and high-K (9/2, 11/2) orbitals interpreting the two SD bands in ^{197}Pb. The $\nu[505]11/2$ orbital was also already excluded from the observed bandhead spin of 9/2. The experimental result clearly shows that the SD bands are built on a $K = 5/2$ orbital, and the comparison with the predictions would prefer the $\nu[752]5/2$ orbital to the $\nu[512]5/2$ one. This assignment is strongly supported by the flatness of the dynamical moment of inertia of the two bands which implies the involvement of an intruder orbital. Therefore we propose that the SD bands in ^{197}Pb are built on the favoured (SD1) and unfavoured (SD2) signatures of the $\nu j_{15/2}[752]5/2$ neutron intruder orbital.

From $(g_K - g_R)K/Q_0$ we can now estimate the quenching α_n of the g_s factor ($\alpha_n = g_s^{\rm eff}/g_s^{\rm free}$). The theoretical values used are: $Q_0 = 19.7$ eb for ^{196}Pb [28], $\langle S_z \rangle = 0.34$ for the $\nu[752]5/2$ orbital, and $g_R = 0.338$ [26]. The extracted g_K factor is $g_K = -0.54 \pm 0.09$ and we derive $\alpha_n = 1.05 \pm 0.17$. This puzzling result for α_n is similar to the other two results obtained in odd-N SD nuclei (^{193}Hg [9] and ^{193}Pb [13,14]): no quenching was found for $g_s^{\rm eff}$ in the neutron SD configurations. This is surprising, especially since the three values concern three different neutron orbitals, $\nu[512]5/2^-$ in ^{193}Hg, $\nu[624]9/2^+$ in ^{193}Pb and $\nu[752]5/2^-$ in ^{197}Pb. This seems to be a difference between neutron and proton SD configurations, the α_p quenching factor for odd-Z SD nuclei being similar to those previously obtained for ND nuclei (≈ 0.6), while $\alpha_n \approx 1$ for odd-N SD nuclei.

5 Conclusion

Thanks to the high efficiency of the EUROBALL IV multidetector array, we have observed cross-talk transitions between the two SD bands in ^{197}Pb. The two SD bands have also been extended to lower frequencies. DCO measurements confirm the $\Delta I = 1$ multipolarity assignment and the extraction of $B(\mathrm{M1})/B(\mathrm{E2})$ ratios leads to a good agreement with the theoretical value obtained by microscopic HF+BCS calculations, interpreting the two bands as built on the two signatures of the $\nu j_{15/2}$ [752]5/2 neutron intruder orbital. The effective spin gyromagnetic factor $g_s^{\rm eff}$ derived in this work appears to be equal to the theoretical $g_s^{\rm free}$ value. This surprising lack of quenching is now the third evidence obtained for neutron SD orbitals, contrary to the results obtained for proton SD orbitals. More precise data of the $B(\mathrm{M1})/B(\mathrm{E2})$ branching ratios are needed, for odd-N and odd-Z nuclei, covering a wider range of nuclei and configurations in order to systematically investigate the quenching of the g-factors and the applicability of the model.

We would like to thank all those involved in the setting up and commissioning of EUROBALL IV. We are also very indebted to the operators of the VIVITRON tandem who have provided us a very stable ^{18}O beam during the six days of the experiment. The work of the Bonn group was supported by BMBF contract no. 06 BN 815.

References

1. M. Girod et al., Phys. Rev. C **38**, 1519 (1988).
2. P. Bonche et al., Nucl. Phys. A **500**, 308 (1989).
3. R.R. Chasman, Phys. Lett. B **219**, 227 (1989).
4. W. Satula et al., Nucl. Phys. A **529**, 289 (1991).
5. S.J. Krieger et al., Nucl. Phys. A **542**, 43 (1992).
6. X-L. Han and C-L. Wu, At. Data Nucl. Data Tables **73**, 43 (1999).
7. M.A. Riley et al., Nucl. Phys. A **512**, 178 (1990).
8. Y. Liang et al., Phys. Rev. C **46**, R2136 (1992).
9. M.J. Joyce et al., Phys. Rev. Lett. **71**, 2176 (1993).
10. W. Reviol et al., Nucl. Phys. A **630**, 434 (1998)..
11. S. Bouneau et al., Phys. Rev. C **53**, R9 (1996).
12. J. Duprat et al., Phys. Lett. B **341**, 6 (1994).
13. L. Ducroux et al., Phys. Rev. C **53**, 2701 (1996).
14. D. Rossbach et al., Nucl. Phys. A **660**, 393 (1999).
15. I.M. Hibbert et al., Phys. Rev. C **54**, 2253 (1996); and in Z. Phys. A **358**, 199 (1997).
16. J. Simpson, Z. Phys A **358**, 139 (1997).
17. I. Deloncle et al., Nucl. Instrum. Meth. Phys. Res. A **357**, 150 (1995).
18. C. Beausang et al., Nucl. Instrum. Meth. Phys. Res. A **364**, 560 (1995).
19. K.S. Krane, Nucl. Data Tables **11**, 407 (1973).
20. G. Baldsiefen et al., Nucl. Phys. A **587**, 562 (1995).
21. S. Perriès et al., Phys. Rev. C **60**, 064313 (1999).
22. J. Becker et al., Phys. Rev. C **46**, 889 (1992).
23. S.M. Harris, Phys. Rev. B **138**, 509 (1965).
24. C.S. Wu et al., Phys. Rev. C **45**, 2507 (1992).
25. L.P. Farris et al., Phys. Rev. C **51**, R2288 (1995).
26. S. Perriès et al., Phys. Rev. C **55**, 1797 (1997).
27. R.H. Mayer et al., Phys. Rev. C **58**, R2640 (1998).
28. U.J. van Severen et al., Phys. Lett. B **434**, 14 (1998).